Original Article

MOLECULAR METABOLISM

Deubiquitinating enzyme USP2 regulates brown adipose tissue thermogenesis via controlling EBF2 stabilization

Yuejie Xu[1,3], Ying Chen[2,3], Ningning Bai[1], Yingying Su[1], Yafen Ye[1], Rong Zhang[1], Ying Yang[1], Caizhi Liu[1,*], Cheng Hu[1,], Jiemin Pan[1,***]**

ABSTRACT

Objective: The activation of brown adipose tissue (BAT) promotes energy expenditure is recognized as a promising therapeutic strategy for combating obesity. The deubiquitinating enzyme family members are widely involved in the process of energy metabolism. However, the specific deubiquitinating enzyme member that affects the BAT thermogenesis remains largely unexplored.

Methods: Adeno-associated virus, lentivirus and small molecule inhibitor were applied to generate USP2 gain- or loss-of-function both *in vivo* and *in vitro*. OxyMax comprehensive laboratory animal monitoring system, seahorse and transmission electron microscopy were used to determine the energy metabolism. Quantitative proteomics, immunofluorescence staining and co-immunoprecipitation were performed to reveal the potential substrates of USP2.

Results: USP2 is upregulated upon thermogenic activation in adipose, and has a close correlation with *UCP1* mRNA levels in human adipose tissue. BAT-specific Usp2 knockdown or systemic USP2 inhibition resulted in impaired thermogenic programs both *in vivo* and *in vitro*. Conversely, overexpression of Usp2 in BAT conferred protection against high-fat diet-induced obesity and associated metabolic disorders. Proteome-wide analysis identified EBF2 as the substrate of USP2 that mediates the thermogenic function of USP2 in BAT.

Conclusions: Our data demonstrated the vital role of USP2 in regulating BAT activation and systemic energy homeostasis. Activation of USP2-EBF2 interaction could be a potential therapeutic strategy against obesity.

Keywords Brown adipose tissue; Thermogenesis; USP2; EBF2; Deubiquitylation

1. INTRODUCTION

Thermogenesis in brown and beige adipocytes protects animals from hypothermia during cold exposure and is associated with resistance to obesity [1—3]. Brown and beige adipocytes are characterized by multilocular lipid droplets and a high density of mitochondria containing uncoupling protein-1 (UCP1) [4]. Upon activation, UCP1 disrupts the mitochondrial membrane potential, facilitating the oxidation of glucose and fatty acids while producing heat as a byproduct [5]. Cold exposure serves as the primary physiological trigger for BAT activation, with β-adrenergic signaling driving processes such as lipolysis, substrate oxidation, and uncoupled respiration [6]. Additionally, an acute nutrient influx, particularly from a high-fat diet (HFD), can activate BAT [7,8]. However, chronic exposure to excess nutrients, as observed in

[1]Department of Endocrinology and Metabolism, Shanghai Diabetes Institute, Shanghai Clinical Center for Diabetes, Shanghai Key Laboratory of Diabetes Mellitus, Shanghai Key Clinical Center for Metabolic Disease, Shanghai Sixth People's Hospital Affiliated to Shanghai Jiao Tong University School of Medicine, Shanghai, 200233, China [2]Jinzhou Medical University Graduate Training Base (Shanghai Sixth People's Hospital Affiliated to Shanghai Jiao Tong University School of Medicine), Jinzhou, 121001, China

[3] Co-first author: Yuejie Xu and Ying Chen.

*Corresponding author. E-mail: adaica@sjtu.edu.cn (C. Liu).

***Corresponding author. E-mail: lilypjm@hotmail.com (J. Pan).

**Corresponding author. E-mail: alfredhc@sjtu.edu.cn (C. Hu).

Abbreviations: BAT, brown adipose tissue; USP2, ubiquitin-specific protease 2; AAV, Adeno-Associated Virus; SVFs, stromal vascular fractions; UCP1, uncoupling protein-; HFD, high-fat diet; DUBs, deubiquitinating enzymes; iWAT, inguinal white adipose tissue; GEO, Gene Expression Omnibus; USP, ubiquitin-specific protease; EBF2, early B cell factor-2; NCD, normal chow diet; OCRs, oxygen consumption rates; CLAMS, Comprehensive Lab Animal Monitoring System; RT-qPCR, Reverse Transcription Quantitative Polymerase Chain Reaction; MOI, multiplicity of infection; i.p., intraperitoneal; cAMP, cyclic AMP; VO2, oxygen consumption; VCO2, carbon dioxide production; GTT, glucose tolerance test; ITT, insulin tolerance test; mtDNA, mitochondrial DNA; OXPHOS, oxidative phosphorylation; FFA, free fatty acid; ALT, alanine aminotransferase; AST, aspartate aminotransferase; Chol, cholesterol; TG, triglycerides; HDL-C, high-density lipoprotein cholesterol; LDL-C, low-density lipoprotein cholesterol; KEGG, Kyoto Encyclopedia of Genes and Genomes; UPS, ubiquitin-proteasome system

Received December 23, 2024 • Revision received March 23, 2025 • Accepted April 1, 2025 • Available online 4 April 2025

https://doi.org/10.1016/j.molmet.2025.102139

obesity, leads to BAT whitening and a subsequent decline in metabolic efficiency. While the mechanisms regulating BAT's thermogenic activity remain inadequately understood, identifying factors that protect thermogenic adipocytes from metabolic stress during adaptation to cold or obesity may hold significant potential for developing therapeutic approaches to treat metabolic diseases.

Ubiquitination and deubiquitination, as a post-translational modification, play crucial roles in regulating protein stability, localization, and function, thus participating in the pathophysiology of various diseases [9,10]. Deubiquitinating enzymes (DUBs) negatively regulate the dynamic and reversible process of ubiquitination by removing ubiquitin molecules from substrate proteins [11,12]. Current research regarding the regulation of adipose function by DUBs primarily focuses on adipogenesis. For instance, the absence of USP19 in stromal vascular fractions (SVFs) of inguinal white adipose tissue (iWAT) fails to promote lipid accumulation and the transcription of adipogenic genes, resulting in improved insulin sensitivity [13]. Additionally, USP7 is crucial in 3T3-L1 cell differentiation and mouse adipose tissue by deubiquitinating acetyltransferase TIP60, which forms a transcriptional co—regulatory complex inducing adipocyte differentiation [14]. USP1 directly interacts with and deubiquitinates C/EBPβ, enhancing its stability in the regulation of adipogenesis [15]. Studies in recent years have revealed the critical role of post-translational regulation in adipose thermogenesis [16,17]. However, little is known about the relationship between DUBs and adipose thermogenesis. Considering the extensive resources of existing Gene Expression Omnibus (GEO) databases, we conducted data mining and identified USP2 as a potentially thermogenesis-related deubiquitinating enzyme.

USP2 belongs to the ubiquitin-specific protease (USP) family. It comprises two primary domains: a catalytic ubiquitin-specific protease domain and a regulatory zinc finger domain [18]. Recent research has underscored the pivotal role of USP2 in regulating cell cycle progression, apoptosis, and protein stability [19]. Moreover, USP2's involvement in metabolic disorders has gradually been revealed, particularly in obesity and type 2 diabetes, where it modulates the stability of lipogenic enzymes and insulin signaling components [20,21]. However, to our knowledge, the detailed role of USP2 in brown adipose tissue thermogenesis remains inadequately explored.

In this study, we investigated the impact of USP2 on thermogenesis using cold exposure mouse models. Mechanistically, we discovered that USP2 interacts with early B cell factor-2 (EBF2), inhibiting its degradation by removing K63-linked ubiquitin from EBF2, thereby maintaining the EBF2-mediated cold adaptation process in BAT. Overall, we revealed a USP2-EBF2 axis in BAT thermogenesis, expanding our understanding of how ubiquitination dynamics influence metabolic adaptations, and identified USP2 as a potential therapeutic target for metabolic diseases.

2. MATERIALS AND METHODS

2.1. Mouse model

All the animal experiments in this study were performed in compliance with protocols approved by Shanghai Sixth People's Hospital Affiliated to Shanghai Jiao Tong University School of Medicine. Mice were allocated to experimental groups randomly. Six to eight-week-old male C57BL/6J mice were purchased from GemPharmatech Co., Ltd (Nanjing, China). Unless otherwise specified, all the mice had free access to food and water and were housed in a temperature- and humidity-controlled (50%), specific pathogen-free animal facility at 22 °C. The animals were housed with 3—5 mice per cage. Mice were maintained on a NCD (P1200F, Shanghai Puluteng Co. Ltd) or a HFD (60% kcal fat; D12492, Research Diets).

2.2. Human adipose tissue samples

Human deep neck fat and paired subcutaneous fat samples were obtained from metabolically healthy patients who underwent thyroidectomy at Shanghai Jiao Tong University Affiliated Sixth People's Hospital. All patients had thyroid-stimulating hormone levels within the normal range, and sample collection was conducted according to previously established protocols [22,23]. This study was approved by the Human Research Ethics Committee of Shanghai Jiao Tong University Affiliated Sixth People's Hospital and Shanghai Seventh People's Hospital. Written informed consent was obtained from each subject.

2.3. Cold exposure test

For the cold tolerance test, 3—4-month-old mice were exposed to cold environments (4 °C) in a climate-controlled rodent incubator (Environmental Cabinet, DBL Co.). Rectal temperature was measured using a thermal probe (Testo925, Testo Inc.).

For chronic cold-exposure experiments, 3—4-month-old mice were kept in the climate-controlled rodent incubator in which temperature was decreased gradually (16 °C for the first 24 h, 10 °C for another 24 h, and 4 °C for the final 24 h).

2.4. Local delivery of adeno-associated virus (AAV) and adenovirus in adipose tissues

Adipocyte-specific adeno-associated virus 2/9 (AAV Serotype 2/9, adiponectin promoter)-mediated overexpression of FLAG-tagged mouse Usp2, control (GFP), shRNA targeting Usp2, and scrambled control (NC) were constructed, amplified, and purified by OBiO Technology (Shanghai, China). A total of 50 μl of $4*10^9$ Vg/μl of each AAV diluted in PBS was injected into the inguinal fat pads or brown fat of mice [24,25]. Adenovirus-mediated overexpression of FLAG-tagged mouse Ebf2 and GFP were constructed, amplified, and purified by HanBio (Shanghai, China). Mice were anesthetized by isoflurane anesthesia (5% induction and 2% maintenance). For AAV delivery in iWAT, AAV was directly injected into the iWAT on either side in multiple spots (5—8 spots per fat pad). For AAV delivery in BAT, the incision site was shaved and disinfected using 70% ethanol. A longitudinal incision at the interscapular region was performed to expose the brown fat as previously reported [25,26]. Virus was bilaterally injected into both lobes of the brown fat and the incisions were sutured after injection. After surgery, all mice received carprofen (5 mg/kg) by intraperitoneal injection. Mice were monitored for changes in body weight, fat mass, cold tolerance, and oxygen consumption, then mice were sacrificed, and tissues were dissected for further analysis.

2.5. Stromal vascular fractions isolation and cell culture

Male C57BL/6J mice aged 6 weeks were euthanized, and SVFs from iWAT and BAT pads were isolated as previously described [27] and maintained in Dulbecco's Modified Eagle Medium: Nutrient Mixture F-12 (DMEM/F12) containing 10% fetal bovine serum (FBS, Gibco). The 2-day post-confluent primary SVFs (designated day 0) were induced in DMEM/F12 containing 10% FBS, 0.5 mM IBMX (Sigma, I7018), 1 μM rosiglitazone (Sigma, R2408), 1 nM T3 (Sigma, T2877), 1 μM dexamethasone (Sigma, D4902) and 5 μg/mL insulin (Lily, HI0240) until day 3. The culture medium was replaced with DMEM/F12 containing 10% FBS, 5 μg/mL insulin, 1 μM rosiglitazone and 1 nM T3 for another four days. On day 6 of differentiation, the cells were ready for further analysis.

2.6. Cell transfection and Co-immunoprecipitation

HEK293T cells were cultured in a 6-well plate in high-glucose DMEM supplemented with 10% FBS and 1% penicillin/streptomycin, and indicated plasmids (3 μg per well) were transfected using EZ Trans (Life-iLab, China). All the plasmids used in this experiment were purchased from Geneppl (Nanjing, China). Cells were harvested and lysed using an immunoprecipitation lysis buffer (Beyotime, P0013). Total proteins were incubated with indicated primary antibodies on a rocking platform overnight at 4 °C. Protein A-agarose (Santa Cruz, sc-2001) was then added to each immunoprecipitation mixture, and incubated at 4 °C for 2 h. The immunoprecipitates were collected and washed three times with cold IP lysis buffer. The agarose was used for western blot analysis.

2.7. Western blots

Cells and tissues were lysed in RIPA lysis buffer (Beyotime Technology, P0013B) containing PMSF (Beyotime Technology, ST506), protease inhibitor cocktail (Roche, 0469311600) and phosphatase inhibitor cocktail (Roche, 04906837001), then subjected to western blot analysis according to the standard protocol. Membranes were incubated overnight at 4 °C with the indicated antibodies. Subsequently the membranes were incubated with secondary antibodies for 1h at room temperature. Protein bands were visualized using the ECL Chemiluminescent Kit (Millipore) on the ChemiDoc Touch Imaging System (Bio-Rad). Image Lab software version 6.0 for acquisition of images from Western blot. ImageJ (National Institutes of Health) version 1.52 for Western blot images densitometry analysis. All antibodies used are summarized in Supplementary Table 1.

2.8. RNA extraction, quantitative PCR, PCR array, and RNA-seq

Total RNA was isolated from cultured cells and tissues by the Trizol reagent (Invitrogen, 15596018). 1 μg of total RNA was then converted to cDNA using the PrimeScript RT reagent Kit (Takara, RR047B). Quantitative real-time PCR (qRT-PCR) amplification were performed with SYBR Green Master Mix (Applied Biosystems) using a QuantStudio Real-Time PCR System (Applied Biosystems) according to the manufacturer's instructions. Quantitative expression of targeted genes was normalized to housekeeping gene 36B4 and calculated using the $2^{-\Delta\Delta CT}$ method. The primer sequences are summarized in Supplementary Table 2.

For RNA-seq, RNA quality was examined with a Nanodrop spectrophotometer (Thermo, MA, USA) and agarose gel electrophoresis. High quality RNA was used to construct library and Illumina NovaSeq6000 was used to perform RNA-seq (Sinotech Genomics, Shanghai, China). Briefly, RNA libraries were constructed by TruSeq® RNA LT Sample Prep Kit v2 (illumina, USA) following the manufacturer's protocol and quantified by Qubit (invitrogen, USA) for cluster generation. Processed RNA-seq data were filtered by removing genes with low read counts. Read counts were normalized using TMM normalization and CPM (counts per million) were calculated to create a matrix of normalized expression values. P value < 0.05 and $|\log_2 FC| > 2$ were used to determine differential genes. KEGG enrichment analysis was performed by KOBAS-i [28].

2.9. Transmission electron microscopy

For BAT, tissue samples were collected from 10-week-old mice exposed to cold stress for 3 d and were cut into pieces of about 1 mm^3 by using a sharp blade. For adipocytes, day-6 differentiated primary adipocytes were obtained following trypsin digestion. Tissue or cell samples were fixed with 2.5% glutaraldehyde in 0.1 M phosphate buffer (pH 7.4) and stored at 4 °C for 3 h. Specimens were then washed using 0.1 M phosphate buffer (pH 7.4), postfixed in 1% OsO4 (pH 7.4) for 2 h at room temperature, dehydrated in ethanol, embedded and baked overnight at 70 °C. Thin sections were obtained using an ultra-microtome (Leica, Germany), stained with 2.6% lead citrate, and examined with a transmission electron microscope (HITACHI, Japan).

2.10. Immunofluorescence

Primary brown adipocytes were cultured on coverslip in 48-well plates and fully differentiated, fixed, permeabilized, and incubated with primary antibodies against USP2 and EBF2 (rabbit anti-USP2, Abgent, AP2131C; sheep anti-EBF2, R&D Systems, AF7006) overnight at 4 °C. Cells were washed and incubated with goat anti-rabbit Alexa Fluor 555 (Abcam, ab150078) and goat anti-sheep Alexa Fluor 488 (Abcam, ab150181) and for 1 h at room temperature. DAPI was used to visualize the nuclei. Images were taken using a Leica confocal microscope and processed using ImageJ.

2.11. Seahorse

Cellular oxygen consumption rates (OCRs) were measured using a XF96 Analyzer (Seahorse Bioscience). Primary adipocytes were differentiated for 6 days and plated at 1000 cells/well in XF 96-well microplates (Seahorse Bioscience) following trypsin digestion. The adherent cells were then transfected with siUsp2 or lenti-OeUsp2 for 48h. Adipocytes were incubated in pre-warmed assay medium (XF base medium with 25 mM glucose, 1 mM sodium pyruvate, 2 mM L-glutamine) for 1 h without CO2 before oxygen consumption analysis. Mitochondrial stress test was measured by injecting the ATP synthase inhibitor oligomycin (1.5 uM), isoproterenol (0.5 uM), the mitochondrial uncoupler carbonyl cyanide4-(trifluoromethoxy) phenylhydrazone (FCCP 2 uM), and the electron transport inhibitor rotenone and antimycin A (0.5 uM) sequentially. The initial OCR values were automatically calculated by Seahorse XF96 software (Wave, Seahorse Bioscience), and the final OCR results were standardized to total protein content in each well.

2.12. MitoTracker staining

The cultured medium of differentiated cells was removed from the dish and 37 °C pre-warmed staining solution containing 100 nM MitoTracker Red probe (Invitrogen) was added into the dish for 30 min under standard growth conditions. Cells images were captured with a fluorescence microscope (Leica) after staining.

2.13. Metabolic assessment

Whole-body fat and lean mass were measured by MRI (MAG-MED AccuFat-1050). Energy expenditure was determined with an OxyMax Comprehensive Laboratory Animal Monitoring System (CLAMs, Columbus Instruments). The mice were acclimated to the system for 48 h before formal testing with free access to food and water throughout the process. Data were analyzed with the CalR analysis software (https://www.CalRapp.org/) [29] and whole-body oxygen consumption was adjusted to lean mass.

2.14. Lentivirus infection

Lentiviral shRNA clones targeting mouse Usp2 and a scrambled control were obtained from Shanghai GeneChem Corporation. For lentivirus production, HEK293T cells were transfected with 8 μg total plasmids, maintaining a ratio of shUsp2: psPAX2: pMD2.G at 4:3:1. After 48 h of incubation, the viral supernatant was collected and concentrated. Mature adipocytes were then transduced with the concentrated virus to knockdown Usp2, using a multiplicity of infection (MOI) of 50. The shRNA sequences are summarized in Supplementary Table 3.

2.15. Insulin and glucose tolerance tests

For glucose tolerance test, mice were fasted overnight and injected intraperitoneally with a glucose solution in saline (1.25 g/kg body weight). For insulin tolerance test, mice received an intraperitoneal injection of insulin at 1.5U/kg body weight. Blood glucose levels were measured at 0, 15, 30, 60, 90 and 120 min after injection with a hand-held glucometer (Accu-Chek glucose reader; Roche).

2.16. Histology and immunohistochemistry

Tissues were fixed in 4% (v/v) formaldehyde in PBS for 24h at 4 °C and embedded in paraffin for histological analysis. Adipose and liver tissues were stained with hematoxylin and eosin (HE) following standard protocols. For immunohistochemistry, the sections were blocked with goat serum, and incubated with rabbit anti-UCP1 (Abcam, ab10983, diluted 1:200) or rabbit anti-USP2 (Abgent, AP2131C, diluted 1:200), followed by incubation with HRP-conjugated goat anti-rabbit (PV-6001, ZSGB-BIO, Beijing, China). The images were acquired by optical microscope (Nikon) using a 20× objective.

2.17. Relative mtDNA analysis

Genomic DNA isolation from adipose or cultured adipocytes was used commercial kits (Qiagen, 158745) according to the manufacturer's protocol. The ratio of mitochondrial DNA (mtDNA) to genomic DNA was measured by performing qPCR. The following primers were used: mt-RNR1: forward 5′-AGGAGCCTGTTCTATAATCGATAAA-3′; reverse 5′-GATGGCGGTATATAGGCTGAA-3′. Mt—ND1: forward 5′- CTAGCA-GAAACAAACCGGGC-3′; reverse 5′- CCGGCTGCGTATTCTACGTT-3′. Genomic RBM15: forward 5′-GGACACTTTTCTTGGGCAAC-3′; reverse 5′-AGTTTGGCCCTGTGAGACAT-3′.

2.18. Quantification and statistical analysis

Statistics were computed with GraphPad Prism 10 software. The statistical details of experiment are indicated in the figure legends. Statistical comparisons between two groups were made by unpaired Student's t-test. Two-way ANOVA with Bonferroni's multiple comparisons was used for comparisons of multiple factors. All data are presented as mean ± standard error of the mean (SEM). $P < 0.05$ was considered as statistically significant, $^{*}P < 0.05$, $^{**}P < 0.01$, $^{***}P < 0.001$.

3. RESULTS

3.1. USP2 expression in adipose is induced by thermogenic stimuli

To identify the changing profile of DUBs associated with the thermogenic process, we analyzed their expression levels in adipose tissue using publicly available transcriptomic data (from the GEO database, accession number GSE86338) during cold exposure in male C57BL/6J mice. Notably, *Usp2* emerged as the candidate gene that significantly upregulated during both BAT thermogenesis activation and iWAT browning (Figure 1A,B). Conversely, transcriptome analysis of the BAT in HFD-induced obese mice and normal diet mice (GSE64718) revealed that *Usp2* was the top downregulated DUBs compared to the normal diet mice (Figure 1C). These results indicate that among the DUBs, USP2 may be involved in regulating adipose browning and thermogenesis.

Next, we set out to examine the involvement of USP2 in BAT function and beige fat recruitment. Of note, we found that USP2 levels are tightly associated with these processes, as the expression of USP2 and UCP1 were increased both in BAT and iWAT in conditions that promoting fat browning, including cold stimulation, CL316,243 treatment and swimming exercise (Figure 1D—G, Figs. S1A—E). In contrast, USP2 was downregulated both in BAT and iWAT of HFD-induced obese mice, as well as mice under thermoneutral environment (Figure 1H,I, Figs. S1F and G). Importantly, we determined the expression of *USP2* and *UCP1* in human subcutaneous and deep neck adipose tissue samples which obtained from patients undergoing thyroidectomy [23]. We observed that the *USP2* and *UCP1* mRNA levels were higher in deep neck adipose tissue compared to the subcutaneous fat, and also showed a close correlation between *USP2* mRNA levels with *UCP1* mRNA levels (Figure 1J,K).

Mature adipocytes are the main drivers of fat browning and thermogenesis. Therefore, we then set out to examine the USP2 expression pattern and found that USP2 was highly expressed in BAT, and then the iWAT and eWAT (Figs. S1H and I). Moreover, USP2 was mainly expressed in mature adipocytes, and could be induced by adrenergic signaling (Figure 1L,M, Figs. S1J—N). Taken together, these results indicate that USP2 may play a previously unappreciated role in regulation of BAT function and beige fat formation.

3.2. USP2 is required for cold-induced thermogenesis

To investigate the potential impact of USP2 on BAT thermogenic function, C57BL/6 mice were administered adeno-associated virus vectors carrying small hairpin RNA-mediated knockdown of Usp2 (AAV-shUsp2) or control sequence (AAV-NC) directly into the BAT (Figure 2A). Usp2 was successfully knocked down in the BAT from AAV-shUsp2 injected mice, as shown by a significant reduction of Usp2 levels compared to controls (Figs. S2A and B). In response to acute cold exposure, mice with BAT-specific Usp2 knockdown ($Usp2^{BKD}$ mice) exhibited significantly lower rectal temperatures, which unanimously exhibited hypothermia (<32 °C) within 3 h (Figure 2B). Infrared imaging further confirmed the inability of $Usp2^{BKD}$ mice to activate BAT thermogenesis and maintain body temperature during cold exposure (Figure 2C). Of note, with Usp2 knockdown in BAT, there was a significant decrease in BAT mass (Figure 2D). Gross examination of BAT revealed a smaller appearance (Figure 2E) and histological analysis revealed dramatically enlarged lipid droplets in $Usp2^{BKD}$ BAT compared to controls (Figure 2F). Further analysis of the cell proliferation and apoptosis revealed that USP2 knockdown had no effect on proliferation but significantly promoted apoptosis compared to the control group (Fig. S2C). To determine the physiological contributions of USP2 in systemic whole-body energy expenditure, we then measured energy expenditure using a comprehensive laboratory animal monitoring system (CLAMS). At ambient temperature, $Usp2^{BKD}$ mice showed reductions in oxygen consumption (VO2), carbon dioxide production (VCO2) and heat production compared to the controls (Figs. S2D—I), and this disparity became even more pronounced upon cold challenge (Figure 2G—L). These were accompanied with blunted ability to induce thermogenic genes (*Ucp1*, *Pgc1α*, *Dio2*, *Adrb3*, *Prdm16* and *Cidea*) expression in BAT of $Usp2^{BKD}$ mice both in cold challenge and ambient temperature (Figure 2M,N, Figs. S2J and K). These results demonstrate that USP2 might be vital for the adaptive thermogenic response of BAT.

3.3. Deficiency of USP2 impairs beige fat formation

We next investigated whether USP2 was required for beige fat formation *in vivo*. Usp2 was knocked down via *in situ* injection of AAV-shUsp2 into the left iWAT pad, while AAV-NC was injected into the right iWAT pad as a control. After three weeks, the mice were subjected to either chronic cold exposure or intraperitoneal injection of CL316,243 (Fig. S3A). Notably, Usp2 deficiency significantly

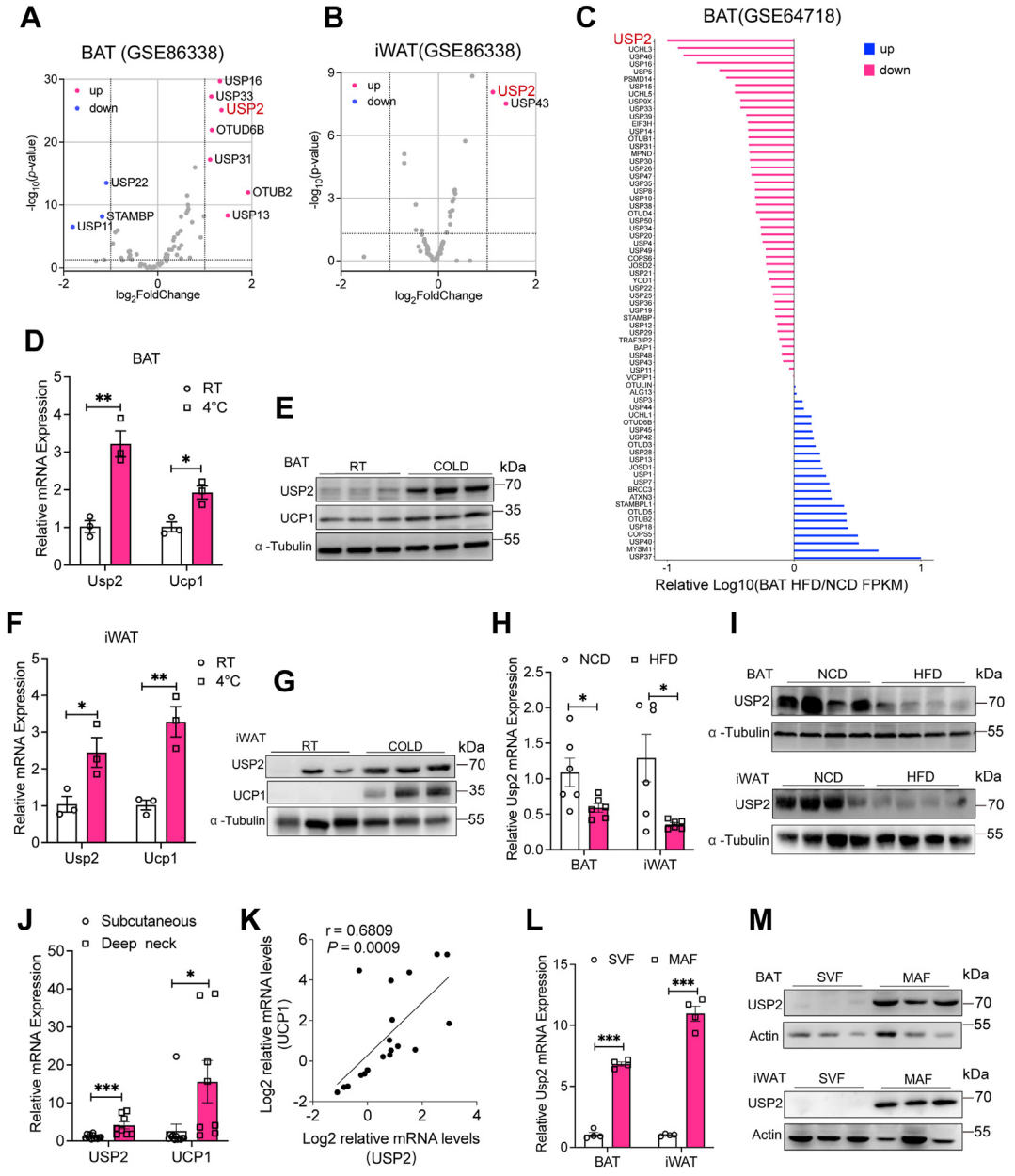

Figure 1: Identification of adipose Usp2 as a potential thermogenic regulator. A. A volcano plot of significantly upregulated (magenta) and downregulated (blue) DUBs in BAT ($n = 70$; 7/3 upregulated/downregulated differentially expressed genes (DEGs)) in 8-week-old C57BL/6 male mice at RT (22 °C) or after 168 h of 4 °C cold exposure, determined by mRNA-seq. Statistically significant DEGs were defined as $P < 0.05$ and $|\log_2$ Foldchange$| > 1$. $n = 3$ animals per temperature condition were analyzed. **B.** A volcano plot of significantly upregulated (magenta) and downregulated (blue) DUBs in iWAT ($n = 72$; 3/0 upregulated/downregulated DEGs) in 16-week-old C57BL/6 male mice at RT (22 °C) or after 168 h of 4 °C cold exposure, determined by mRNA-seq. Statistically significant DEGs were defined as $P < 0.05$ and $|\log_2$ Foldchange$| > 1$. $n = 2$ animals per temperature condition were analyzed. **C.** The bar graph of upregulated (blue) and downregulated (magenta) DUBs in BAT in C57BL/6 male mice fed normal diet or high-fat diet for 20 weeks, determined by mRNA-seq. $n = 3$ animals per dietary condition were analyzed. **D.** Quantitative PCR analysis of Usp2 in BAT of 8-week-old C57BL/6 male mice at RT (22 °C) ($n = 3$) or exposed to cold (4 °C) for 3 days ($n = 3$). **E.** Immunoblot analysis of USP2 in BAT of 8-week-old C57BL/6 male mice at RT (22 °C) ($n = 3$) or exposed to cold (4 °C) for 3 days ($n = 3$). **F.** Quantitative PCR analysis of Usp2 in iWAT of 8-week-old C57BL/6 male mice at RT (22 °C) ($n = 3$) or exposed to cold (4 °C) for 3 days ($n = 3$). **G.** Immunoblot analysis of USP2 in iWAT of 8-week-old C57BL/6 male mice at RT (22 °C) ($n = 3$) or exposed to cold (4 °C) for 3 days ($n = 3$). **H.** Quantitative PCR analysis of Usp2 in BAT and iWAT of C57BL/6 male mice fed a HFD ($n = 6$) or NCD ($n = 6$) for 16 weeks. **I.** Immunoblot analysis of USP2 in BAT and iWAT of C57BL/6 male mice fed a HFD ($n = 4$) or NCD ($n = 4$) for 16 weeks. **J.** Quantitative PCR analysis of Usp2 and Ucp1 in human deep neck fat ($n = 8$) and subcutaneous fat ($n = 12$). **K.** The scatter plot illustrates the relationship between the relative expression of USP2 and UCP1 in human deep neck adipose tissue ($n = 8$) compared to subcutaneous adipose tissue ($n = 12$). **L.** Quantitative PCR analysis of Usp2 in mature adipocytes and SVFs of BAT and iWAT of 8-week-old C57BL/6 male mice ($n = 4$). **M.** Immunoblot analysis of USP2 in mature adipocytes and SVFs of BAT and iWAT of 8-week-old C57BL/6 male mice ($n = 3$). For statistical analysis, Spearman correlation analysis with 95% confidence interval was performed in K. Unpaired, two-tailed *t*-tests were performed in D, F, H, J and L. ($^*P < 0.05$, $^{**}P < 0.01$, $^{***}P < 0.001$). Each point represents a biological replicate. Data were presented as the mean ± S.E.M. (For interpretation of the references to color in this figure legend, the reader is referred to the Web version of this article.)

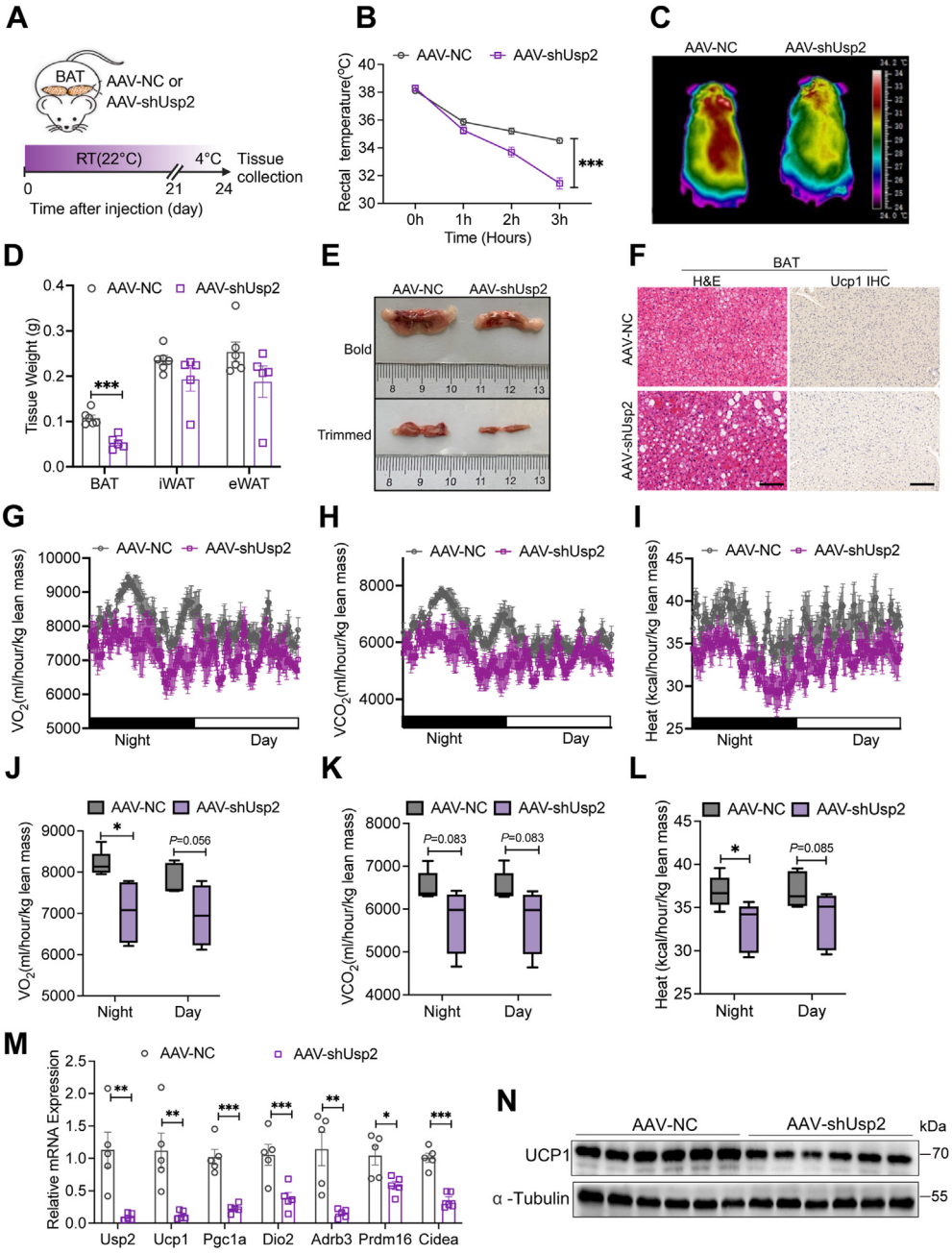

Figure 2: Usp2 ^{BKD} mice exhibit defective energy expenditure and thermogenesis. A. Schematic diagram of the in-situ injection of AAV-shUsp2 into BAT for the establishment of the Usp2^{BKD} model. Image created with BioRender.com. **B.** Rectal temperature of Usp2^{BKD} vs control mice during acute cold exposure. Usp2^{BKD} vs control, ($n = 10$ vs 8). **C.** Representative infrared images of Usp2^{BKD} and control mice following 4 h of acute cold exposure. **D.** Adipose tissue weights of Usp2^{BKD} and control mice. Usp2^{BKD} vs control, ($n = 4$ vs 6). **E.** Representative photographs of BAT of Usp2^{BKD} and control mice. **F.** Representative H&E staining and UCP1 immunostaining of BAT (Scale bar, 100 μm). **G-I.** Oxygen consumption rate (**G**), carbon dioxide production rate (**H**) and heat production rate (**I**) of Usp2^{BKD} and control mice over 24-hour period monitored at cold (4 °C). Usp2^{BKD} vs control, ($n = 4$ vs 5). **J-L.** Average oxygen consumption rate (**J**), average carbon dioxide production rate (**K**) and average heat production rate (**L**) at day time or night time during the 24-hour of monitoring as in (**G-I**). **M.** Quantitative PCR analysis of Usp2 and thermogenic genes in BAT of Usp2^{BKD} and control mice exposed to cold (4 °C) for 3 days ($n = 5$). **N.** Immunoblot analysis of UCP1 in BAT of Usp2^{BKD} and control mice exposed to cold (4 °C) for 3 days. For statistical analysis, two-way ANOVA was performed in B and G-I. Unpaired, two-tailed *t*-tests were performed in D and J-M. ($^*P < 0.05$, $^{**}P < 0.01$, $^{***}P < 0.001$). Each point represents a biological replicate. Data were presented as the mean ± S.E.M.

diminished the effect of cold exposure or CL316,243 on beige fat formation in iWAT, as shown by iWAT mass (Figs. S3B—D), histological examination (Fig. S3E), and RT-qPCR analysis of thermogenic genes expression (Figs. S3F—H). These findings collectively indicate that USP2 is essential for mediating beige fat formation in response to cold exposure and β_3-adrenergic stimulation.

3.4. Pharmacological inhibition of USP2 suppresses thermogenesis

To have a better understanding of the *in vivo* role of USP2 on metabolic performances from a systemic point of view, we treated C57BL/6 mice with ML364, a selective chemical inhibitor of USP2 [30] (Figure 3A). Three weeks of treatment did not significantly impact body weight, liver weight, serum ALT and AST, and serum lipid-related indexes

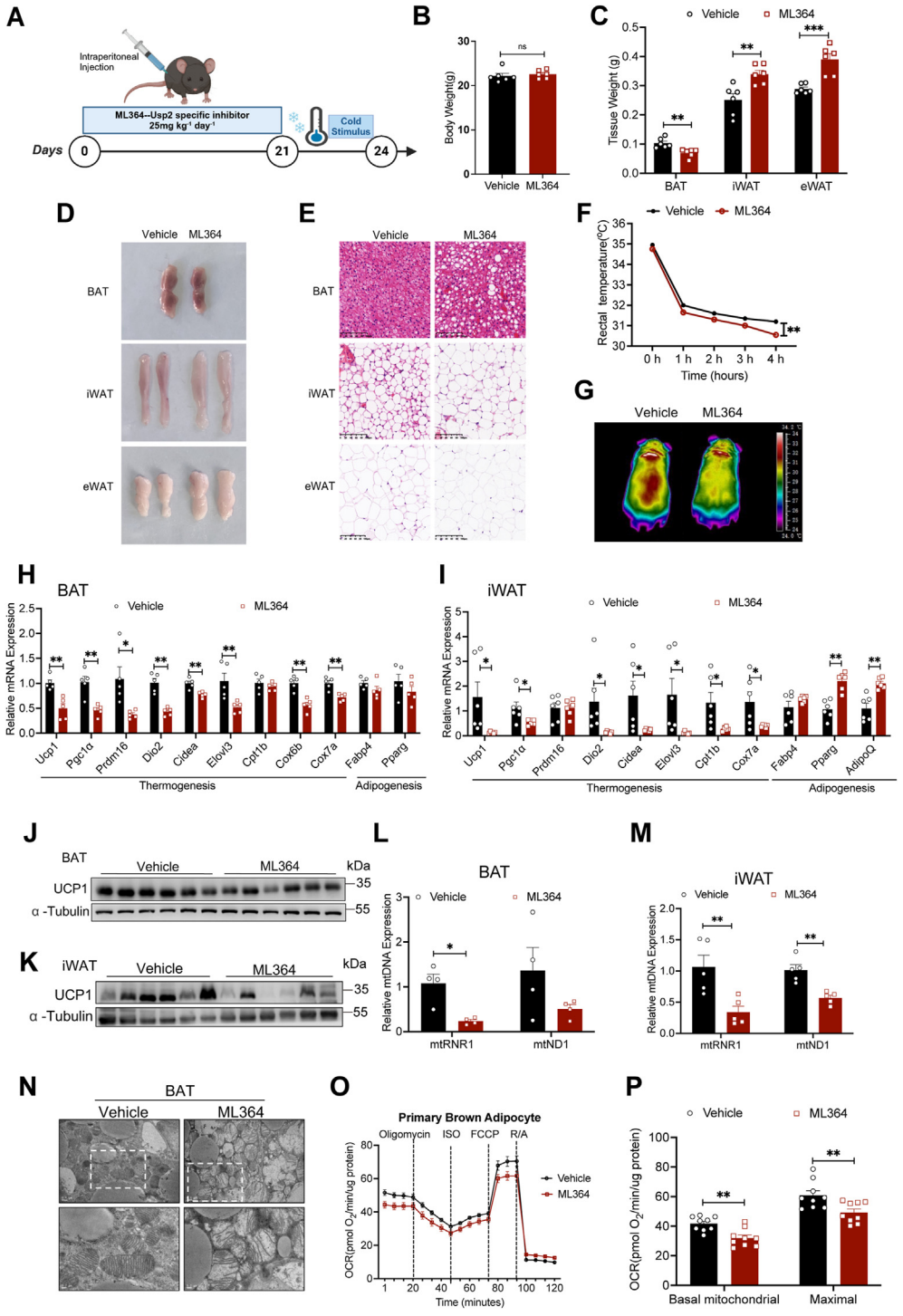

Figure 3: Pharmacological inhibition of USP2 suppresses thermogenesis *in vivo* and *in vitro*. **A.** Schematic diagram of intraperitoneal injection of ML364, followed by cold exposure for 3 days. **B.** Body weight of mice ($n = 6$). **C.** Tissue weight of the indicated tissue in mice treated with ML364 or vehicle ($n = 6$). **D.** Representative photographs of adipose tissue in mice treated with ML364 or vehicle. **E.** Representative H&E staining of adipose tissue in mice treated with ML364 or vehicle. **F.** Rectal temperature of mice treated with ML364 or vehicle during acute cold exposure ($n = 10$). **G.** Representative infrared images of mice treated with ML364 or vehicle following 4 h of acute cold exposure. **H.** Quantitative PCR analysis of thermogenic and adipogenic genes of BAT in mice treated with ML364 or vehicle ($n = 5$). **I.** Quantitative PCR analysis of thermogenic and adipogenic genes of iWAT in mice treated with ML364 or vehicle ($n = 6$). **J.** Immunoblot analysis of UCP1 of BAT in mice treated with ML364 or vehicle ($n = 6$). **K.** Immunoblot analysis of UCP1 of iWAT in mice treated with ML364 or vehicle ($n = 6$). **L.** Mitochondrial DNA levels of BAT in mice treated with ML364 or vehicle ($n = 4$). **M.** Mitochondrial DNA levels of iWAT in mice treated with ML364 or vehicle ($n = 5$). **N.** Representative TEM images of mitochondria of BAT in mice treated with ML364 or vehicle. **O.** OCRs of primary brown adipocytes pretreated with ML364 or vehicle ($n = 9$). **P.** Bar graphs represent quantification of basal and maximal oxygen consumption of the OCRs in O. For statistical analysis, two-way ANOVA was performed in F. Unpaired, two-tailed *t*-tests were performed in B, C, H, I, L, M and P. ($^*P < 0.05$, $^{**}P < 0.01$, $^{***}P < 0.001$). Each point represents a biological replicate. Data were presented as the mean ± S.E.M. (For interpretation of the references to color in this figure legend, the reader is referred to the Web version of this article.)

(Figure 3B and Figs. S4A—C). However, ML364-treated mice showed less BAT mass, but higher weights of iWAT and eWAT compared to controls (Figure 3C,D). H&E staining indicated augmented lipid deposition and a transition from small to large lipid droplets in the adipose tissue of ML364-treated mice, with comparable hepatic morphology (Figure 3E and Fig. S4D). Furthermore, following acute cold exposure, ML364-treated mice presented significantly lower rectal and surface temperatures (Figure 3F,G). These were accompanied with significant decreased expression of thermogenic-related genes in both BAT and iWAT of ML364-treated mice, and no changes were observed in general markers for adipogenesis in BAT, which increased in iWAT (Figure 3H—K).

Finally, we investigated the probability of mitochondrial dysfunction in BAT and iWAT of ML364-treated mice. As expected, mitochondrial DNA (mtDNA) content was significantly reduced in both BAT and iWAT of ML364-treated mice (Figure 3L,M). Consistently, transmission electron microscopy revealed aberrant mitochondrial structure in the BAT of ML364-treated mice, as shown by enlarged mitochondria with disorganized cristae structures in BAT compared to vehicle-treated mice (Figure 3N).

On the other hand, we also studied the effects of ML364 on differentiated primary brown adipocytes. ML364 treatment led to a time and dose -dependent reduction in UCP1 protein level without signs of cytotoxicity (Figs. S4E—G). Moreover, the mRNA expression of genes that critical to the thermogenic program in adipocytes were diminished in cells treated with ML364 (Fig. S4H). Notably, further examination of OCRs showed significant inhibition of both basal and maximal respiration in ML364-treated cells compared to vehicle-treated controls (Figure 3O,P), with markedly reduced levels of mitochondrial electron transport chain proteins in adipocytes, including ATP5A, SDHB, and NDUFB8 (Fig. S4I). Moreover, the MitoTracker staining and mtDNA analysis revealed a reduction in mitochondrial number in ML364-treated adipocytes compared to controls (Figs. S4J and K). Collectively, these data suggested an indispensable role of USP2 in beige fat function and adaptive thermogenic activation.

3.5. USP2 acts cell-autonomously to modulate adipocyte thermogenic activation

To further evaluate the effect of USP2 on thermogenic activation in adipocytes, we knocked down Usp2 in mature primary brown adipocytes. Differentiated primary brown adipocytes were transfected with either a control lentivirus or a shUsp2 lentivirus for 60 h and the cells were collected for RNA-seq analysis (Figure 4A). Kyoto Encyclopedia of Genes and Genomes (KEGG) analysis revealed that this category is significantly enriched in metabolic pathways, fatty acid metabolism, oxidative phosphorylation, and adaptive thermogenesis (Figure 4B). We examined the expression patterns of 254 previously reported BAT-specific genes [31] and found that 41 of these were significantly downregulated in the Usp2 knockdown group (Figure 4C). Of note, knockdown of Usp2 greatly reduced the expression of thermogenic genes, while there were no significant differences in mRNA levels of mature adipocyte-related genes (*Fabp4*, *AdipoQ*, *Pparg* and *Glut4*) (Figure 4D,E).

These findings prompted us to investigate whether mitochondrial function is compromised due to the deficiency of Usp2. Indeed, RT-qPCR analysis confirmed that mitochondrial-related genes, including *Mfn1*, *Mfn2*, and *Tfam* were inhibited with Usp2 knockdown (Figure 4F). MitoTracker Red staining and mtDNA content analysis indicated a decreased mitochondrial number in Usp2 knockdown adipocytes compared to controls (Figure 4G,H). Importantly, the mitochondrial stress test showed that Usp2-knockdown adipocytes exhibited lower UCP1-dependent and maximal respiration compared to the control adipocytes (Figure 4I,J). Furthermore, Usp2-knockdown adipocytes contained dysmorphic mitochondria with sparse and distended cristae, the principal sites of oxidative phosphorylation (OXPHOS) complexes at the ultrastructural level (Figure 4K). In consistent, analysis of OXPHOS protein expression in Usp2-knockdown adipocytes showed a marked decrease in OXPHOS complex I, II and IV (Figure 4L,M).

To complement the loss-of-function model of Usp2, we subsequently overexpressed Usp2 via lentivirus (OeUsp2) in mature primary brown adipocytes. Overexpression of Usp2 in brown adipocytes elevated mRNA and protein levels of thermogenic and mitochondrial genes, with no changes in the expression of common adipose markers (Figs. S5A and B). Consistently, the OeUsp2 adipocytes displayed a significantly higher OCRs at both uncoupled respiration and maximal respiration (Figs. S5C and D). In addition, enhanced fluorescence intensity in MitoTracker Red staining in the OeUsp2 adipocytes indicated an increased mitochondrial number (Fig. S5E). Taken together, these results suggest that USP2 modulates thermogenic activation in brown adipocytes in a cell-autonomous manner.

3.6. BAT-specific overexpression of USP2 promotes thermogenesis and improves HFD-induced obesity

Given that decreased levels of USP2 inhibits thermogenic metabolism in adipose tissues, we hypothesized that USP2 overexpression might have therapeutic potential for obesity-associated metabolic dysfunction. To test this hypothesis, AAV mediated Usp2 overexpression (AAV-OeUsp2) or a control (AAV-GFP) was administered into the BAT of C57BL/6 mice, followed by HFD feeding (Figure 5A). The AAV-mediated FLAG-tagged Usp2 overexpression system functioned effectively in the BAT of injected mice, producing significantly and consistently elevated Usp2 expression levels (Figs. S6A and B). As expected, mice with USP2 overexpression ($Usp2^{BOE}$ mice) gained less weight upon HFD feeding compared to control mice (Figure 5B). Body composition analysis revealed that the overexpression of USP2 decreased fat mass while exhibiting no detectable effect on lean mass (Figure 5C). Consistently, the tissue weights of iWAT and epididymal white adipose tissue (eWAT) were markedly decreased in $Usp2^{BOE}$ mice (Figure 5D). Additionally, HFD-fed $Usp2^{BOE}$ mice displayed enhanced thermogenesis and energy expenditure, as shown by elevated body core and surface body temperatures upon cold challenge (Figure 5E,F). Histological analysis revealed a substantially reduced proportion of larger adipocytes in BAT, increased proportion of larger adipocytes in iWAT and eWAT, along with less lipid accumulation in the liver in $Usp2^{BOE}$ mice (Figure 5G). Notably, the BAT of $Usp2^{BOE}$ mice exhibited enhanced expression of thermogenic genes (Figure 5H), with increased UCP1 immunohistochemical staining compared to the control group (Figure 5I). In terms of systemic energy expenditure, the CLAMS study indicated that $Usp2^{BOE}$ mice exhibited significantly escalated oxygen consumption, CO_2 emission, and heat production (Figure 5J—O, Figs. S6C—E). Further glucose tolerance test (GTT) and insulin tolerance test (ITT) demonstrated that upregulation of USP2 levels in BAT of mice improved both glucose tolerance and insulin sensitivity (Figure 5P—S). Collectively, these results confirm that BAT-specific overexpression of USP2 alleviates diet-induced metabolic disorders by promoting brown fat thermogenesis and whole-body energy expenditure.

3.7. Identification of EBF2 as the substrate protein of USP2

As a DUB, USP2 functions by removing ubiquitin from substrate proteins. We hypothesized that it might influence the thermogenic process through post-translational modifications of downstream genes. To identify the substrates of USP2 in brown adipose tissue, we conducted

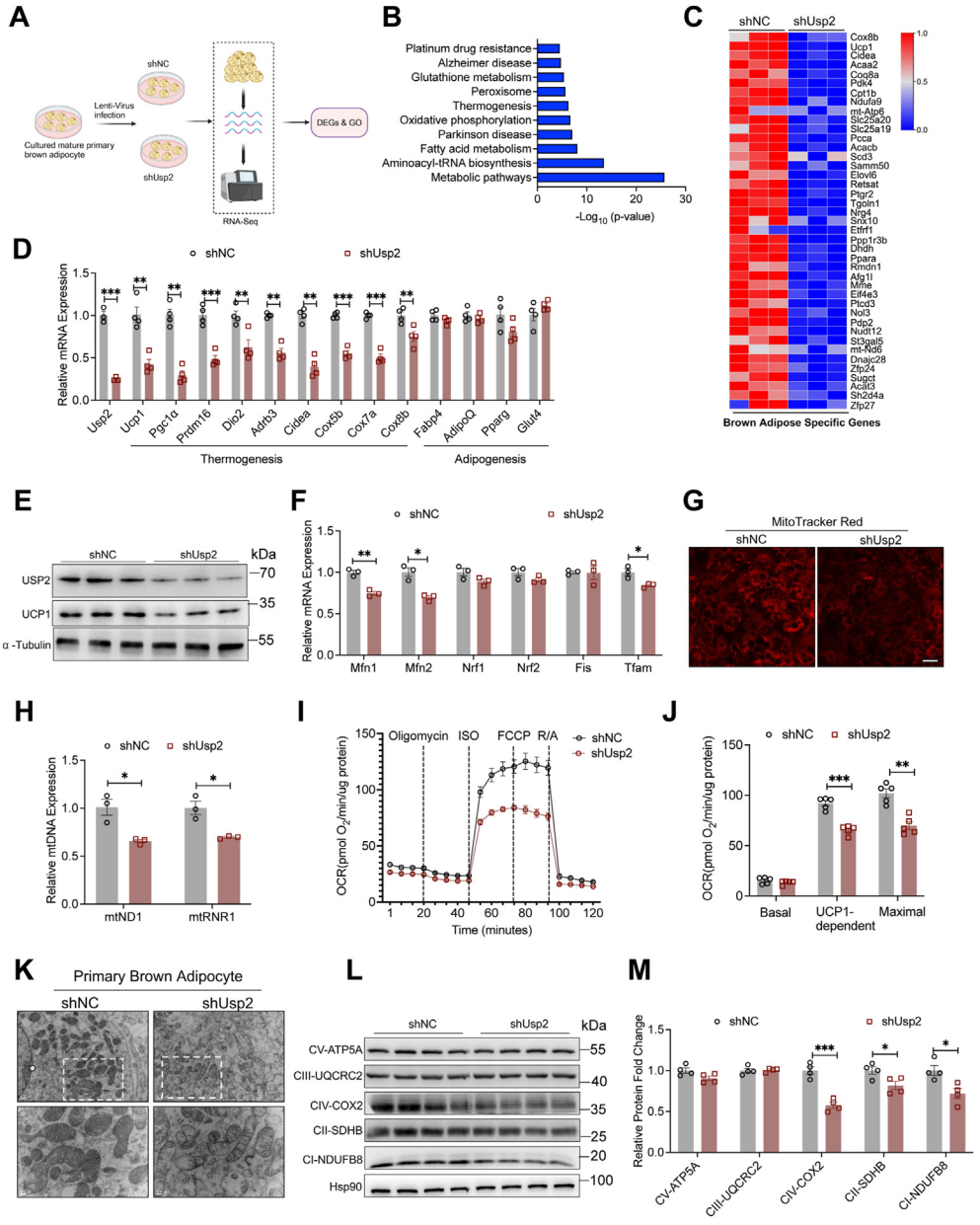

Figure 4: Depletion of USP2 cell-autonomously inhibits adipocyte thermogenic metabolism.
A. Schematic diagram of transcriptional profiling analysis in mature brown primary adipocytes transfected with shUsp2 lentivirus. Image created with BioRender.com. **B.** Top significantly downregulated KEGG pathways, on the basis of RNA-seq data ($n = 3$). **C.** Profile of transcript levels of differentially expressed BAT-specific genes in Usp2 knockdown or control adipocytes. **D.** Quantitative PCR analysis of thermogenic and adipogenic genes in Usp2 knockdown or control adipocytes ($n = 4$). **E.** Immunoblot analysis of UCP1 in Usp2 knockdown or control adipocytes ($n = 3$). **F.** Quantitative PCR analysis of mitochondrial genes in Usp2 knockdown or control adipocytes ($n = 3$). **G.** Representative fluorescent images of MitoTracker staining of Usp2 knockdown or control adipocytes (Scale bar, 400 μm). **H.** Mitochondrial DNA levels of Usp2 knockdown or control adipocytes ($n = 3$). **I.** Oxygen consumption rates of Usp2 knockdown or control adipocytes ($n = 6$). **J.** Bar graphs represent quantification of basal and maximal oxygen consumption of the OCRs in I. **K.** Representative TEM images of mitochondria in Usp2 knockdown or control adipocytes. **L.** Immunoblot analysis of OXPHOS protein expression in Usp2 knockdown or control adipocytes ($n = 4$). **M.** Quantification of the immunoblots in L. For statistical analysis, unpaired, two-tailed *t*-tests were performed in D, F, H, J and M. ($^{*}P < 0.05$, $^{**}P < 0.01$, $^{***}P < 0.001$). Each point represents a biological replicate. Data were presented as the mean ± S.E.M. (For interpretation of the references to color in this figure legend, the reader is referred to the Web version of this article.)

quantitative proteomics analysis on BAT from cold-stimulated Usp2^{BKD}mice and control mice (Figure 6A). A total of 306 proteins were downregulated, while 110 proteins were upregulated in Usp2 knockdown brown adipose tissue compared to the control group (Figure 6B). Subsequent KEGG pathway analysis revealed that the downregulated proteins were predominantly enriched in metabolic pathways (Figure 6C). Intriguingly, we noticed that there were 16 proteins that were completely absent in the Usp2 knockdown BAT (Figure 6D). Among these proteins, EBF2 has been demonstrated as the pivotal regulatory role in the development of brown adipose and adaptive thermogenesis [32], which piqued our interest.

Indeed, RT-qPCR and western blot analysis of EBF2 showed that the protein levels of EBF2 were significantly decreased in the Usp2 knockdown BAT compared to controls, with comparable mRNA levels

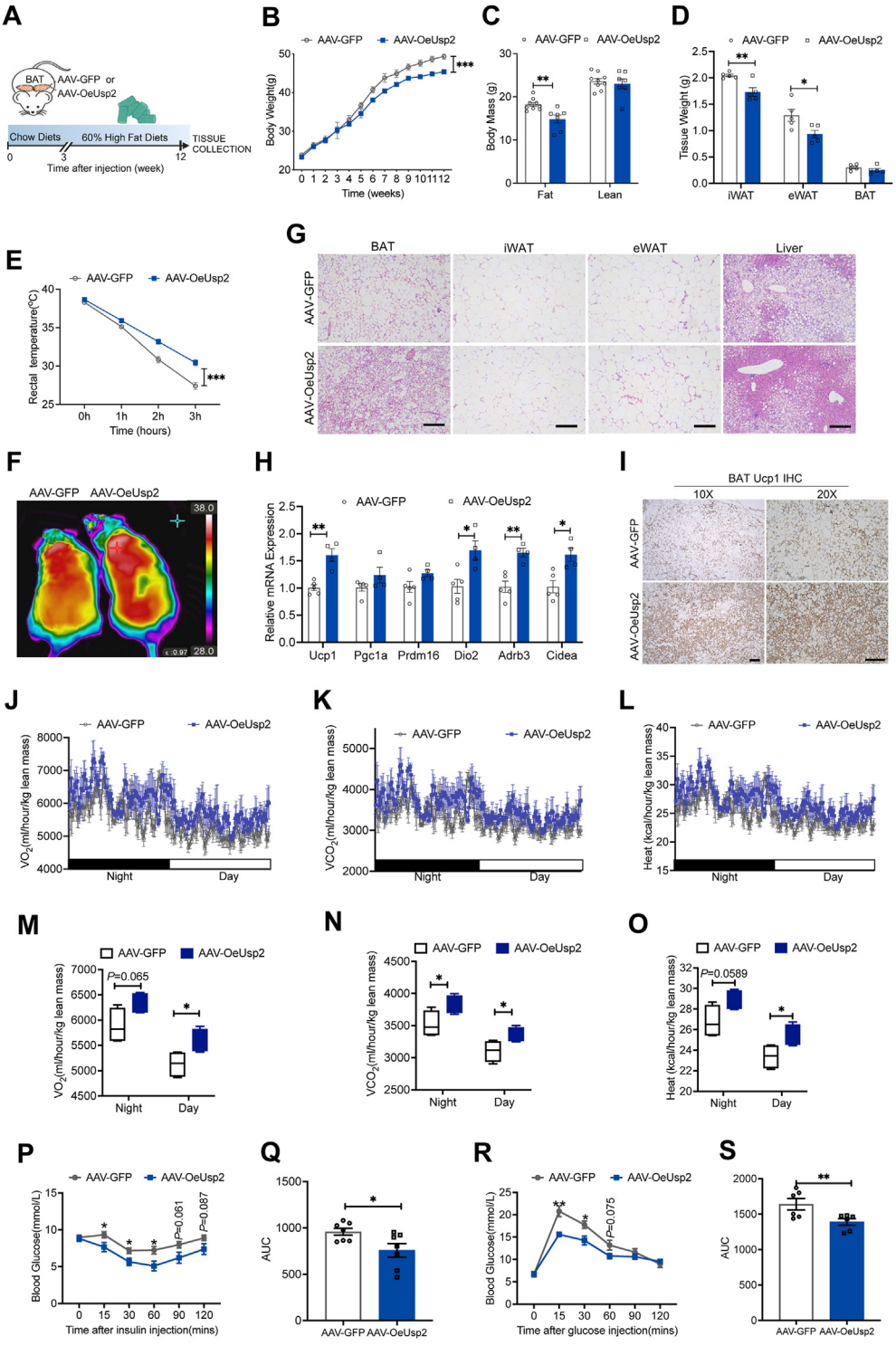

Figure 5: Overexpression of Usp2 in BAT ameliorates HFD-induced obesity and metabolic dysfunction. A. Schematic diagram of the in-situ injection of AAV-OeUsp2 into BAT for the establishment of the Usp2^{BOE} model, followed by HFD feeding. **B.** Body weight of Usp2^{BOG} and control mice housed at RT (22 °C). Usp2^{BOE} vs control, ($n = 5$ vs 6). **C.** Lean mass and fat mass. Usp2^{BOE} vs control, ($n = 7$ vs 9). **D.** The weight of indicated tissues ($n = 5$). **E.** Rectal temperature of Usp2^{BOE} and control mice during acute cold exposure ($n = 8$). **F.** Representative infrared images of Usp2^{BOE} and control mice following 4 h of acute cold exposure. **G.** Representative H&E staining of adipose tissue and liver in Usp2^{BOE} and control mice (Scale bar, 100 μm). **H.** Quantitative PCR analysis of thermogenic genes in BAT of Usp2^{BOE} and control mice. Usp2^{BOE} vs control, ($n = 4$ vs 5). **I.** Representative Ucp1 immunostaining of BAT in Usp2^{BOE} and control mice (Scale bar, 100 μm). **J-L.** Oxygen consumption rate (**J**), carbon dioxide production rate (**K**) and heat production rate (**L**) of Usp2^{BOE} and control mice over 24-hour period monitored at RT (22 °C) ($n = 4$). **M-O.** Average oxygen consumption rate (**M**), average carbon dioxide production rate (**N**) and average heat production rate (**O**) at day time or night time during the 24-hour of monitoring as in (J–L). **P.** Insulin tolerance test (ITT) results of mice after 8 weeks of HFD feeding ($n = 7$). **Q.** Analysis of ITT results in P. **R.** Glucose tolerance test (GTT) results of mice after 8 weeks of HFD feeding ($n = 6$). **S.** Analysis of GTT results in R. For statistical analysis, two-way ANOVA was performed in B, E, J-L, P and R. Unpaired, two-tailed *t*-tests were performed in C, D, H, M–O, Q and S. ($^*P < 0.05$, $^{**}P < 0.01$, $^{***}P < 0.001$). Each point represents a biological replicate. Data were presented as the mean ± S.E.M.

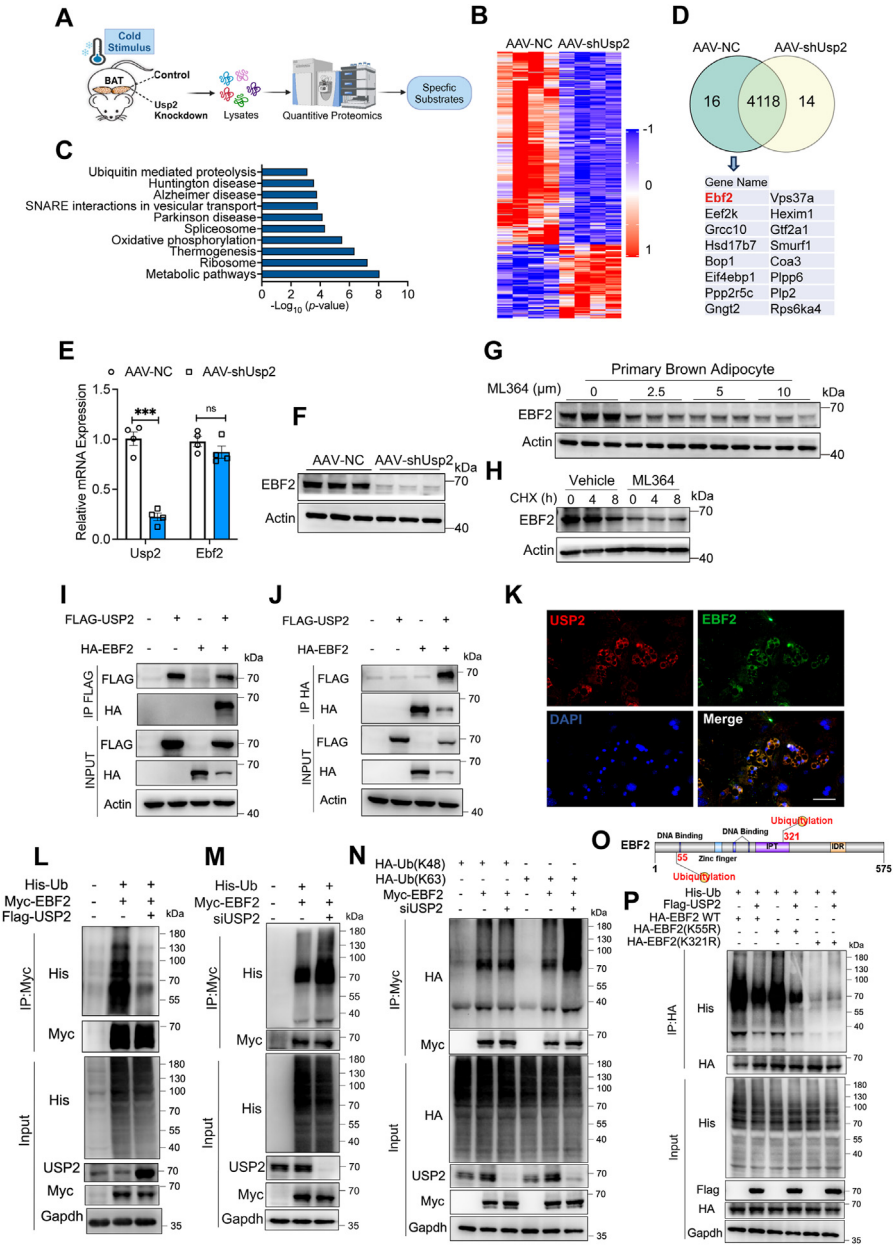

Figure 6: USP2 stabilizes EBF2 by removing K63-linked polyubiquitination at the K321 site of EBF2. A. Schematic illustration of a quantitative proteomic screen to identify proteins binding to USP2 in brown adipose. **B.** Heatmaps representing the upregulated and downregulated genes in BAT, assessed by quantitative proteomics ($n = 4$) (Fold change>2.0 and P value < 0.05). **C.** Top significantly downregulated KEGG pathways, on the basis of quantitative proteomic data. **D.** Venn diagram showing proteins consistently present in control group while consistently absent in USP2 knockdown group. **E.** Quantitative PCR analysis of EBF2 in USP2 knockdown BAT ($n = 4$). **F.** Immunoblot analysis of EBF2 protein expression in USP2 knockdown BAT ($n = 3$). **G.** Immunoblot analysis of EBF2 protein expression in primary brown adipocytes treated with varying doses of ML364. **H.** Immunoblot analysis of EBF2 protein expression in primary brown adipocytes pretreated with ML364 (2.5 μM) for 24 h, followed by cycloheximide (25 μg/mL) treatment for the indicated time. **I-J.** Co-IP analysis of association of USP2 with EBF2 in HEK293T cells co-transfected with Flag-labeled USP2 and HA-labeled EBF2 plasmids. **K.** Representative immunofluorescence in primary brown adipocytes: Nuclei was stained with DAPI in blue, USP2 was stained in red, and EBF2 was stained in green (Scale bar, 100 μm). **L.** Immunoblot analysis of indicated proteins in HEK293T cells co-transfected with Myc-labeled EBF2 and His-Ub in the presence of vector or Flag-labeled USP2 plus the proteasome inhibitor MG132 (10 μM) for 2 h before IP of whole cell lysates with Myc magnetic beads. **M.** Immunoblot analysis of indicated proteins in HEK293T cells co-transfected with Myc -labeled EBF2 and His-Ub in the presence of siControl or siUsp2 plus MG132 for 2 h before IP of whole cell lysates with Myc magnetic beads. **N.** Immunoblot analysis of the indicated proteins in HEK293T cells co-transfected with Myc-labeled EBF2 and HA-K48-Ub or HA-K63-Ub in the presence of siControl or siUsp2 plus MG132 for 2 h before IP of whole cell lysates with Myc magnetic beads. **O.** Schematic illustration of the construct for mutating the ubiquitinated lysine residue of EBF2. **P.** Immunoblot analysis of the indicated proteins in HEK293T cells co-transfected with Flag-labeled USP2 and His-Ub in the presence of HA-EBF2, HA-EBF2-K55R or HA-EBF2-K321R for 24 h plus MG132 for 2 h before IP of whole cell lysates with HA magnetic beads. For statistical analysis, unpaired, two-tailed t-test was performed in E. (***$P < 0.001$). Each point represents a biological replicate. Data were presented as the mean ± S.E.M. (For interpretation of the references to color in this figure legend, the reader is referred to the Web version of this article.)

of *Ebf2* (Figure 6E,F). Furthermore, ML364 treatment resulted in a dose-dependent reduction in the protein levels of EBF2 (Figure 6G). Of note, cycloheximide enhanced the degradation of EBF2 protein as USP2 was inhibited by ML364 (Figure 6H). To further determine the interaction between USP2 and EBF2, we constructed Flag-USP2 and HA-EBF2 plasmids and transfected them individually or together into HEK293T cells. The association between Flag-USP2 and HA-EBF2 was detected in these cells (Figure 6I,J). Moreover, immunofluorescence staining confirmed the interaction of USP2 and EBF2 in primary brown adipocytes (Figure 6K).

Next, we set out to unravel the mechanism of USP2 regulating the deubiquitination of EBF2. To achieve this, we co-overexpressed Myc-tagged EBF2 and His-tagged ubiquitin in HEK293T cells, and transfected with either Usp2 siRNA or Usp2 overexpression plasmid. Western blot analysis showed increased total EBF2 ubiquitination in Usp2-deficient cells and decreased EBF2 ubiquitination levels in Usp2 overexpression cells (Figure 6L,M). Furthermore, we used ubiquitin protein mutants with all lysine residues except K48, K63 replaced by arginine to identify the ubiquitin chain type of EBF2 removed by USP2. Western blot analysis showed that the K63-linked but not K48-linked ubiquitin chain was the major form removed by USP2 (Figure 6N). Computational predictions suggested that EBF2 contains two ubiquitination sites, specifically at K55 and K321 (Figure 6O). Consequently, we constructed mutant plasmids targeting these two ubiquitination sites, and western blot analysis showed that the total polyubiquitination of EBF2-K321R was significantly lower than EBF2-WT and was not further reduced by Usp2 overexpression in HEK293T cells (Figure 6P). Therefore, these findings indicate that USP2 targets K63 polyubiquitination of EBF2 at the K321 site, and controls the protein stability of EBF2.

3.8. EBF2 overexpression attenuates USP2 deficiency-induced thermogenic dysfunction

To examine the role of EBF2 in mediating the metabolic functions of USP2 in BAT, C57BL/6 mice were local injection of AAV-shUsp2 or AAV-NC in BAT, and then the adenovirus mediated EBF2 (Adv-EBF2) or GFP (Adv-GFP) overexpression were administrated in BAT 21 days after the AAV injection (Figure 7A). Both qPCR and Western blot results demonstrated that Usp2 was efficiently silenced while EBF2 was successfully overexpressed in the experimental groups (Figs. S7A and B). As expected, USP2 deficiency in brown adipose resulted in reduced BAT weight and a substantially increased proportion of larger adipocytes compared to control mice, while this morphological transformation was abolished by the overexpression of EBF2 in brown adipose tissue (Figure 7B—D). Consistently, both immunohistochemistry and immunoblotting analyses showed that UCP1 abundance was lower in Usp2 knockdown mice compared to controls, which was rebounded by overexpression of EBF2 (Figure 7E,F). Meanwhile, overexpression of EBF2 in brown adipose dulled the inhibitory effect of adipose USP2 deficiency on the mRNA expression of thermogenic genes including *Ucp1*, *Dio2*, *Adrb3* and *Cidea* (Figure 7G). Notably. BAT-specific overexpression of EBF2 reversed the suppression of VO2, VCO2, and heat production caused by USP2 deficiency (Figure 7H—M). Overall, these findings suggest a critical role for USP2 in regulating BAT function and whole-body energy homeostasis, potentially via controlling the protein stability of EBF2.

4. DISCUSSION

Post-translational modifications play an important role in maintaining protein homeostasis through controlling subcellular localization, stability, and activity of a modified protein. The ubiquitylation—deubiquitylation axis is one of the major post-translational modifications that regulates protein stability. However, considerable progress has been made in understanding the transcriptional networks that drive thermogenic activation in BAT, there remains a significant knowledge gap regarding the role of post-translational modifications in sustaining BAT thermogenesis. The main finding of this study is the identification of the key deubiquitination regulatory protein USP2 in the process of fat thermogenesis.

Upon thermogenic activation, BAT undergoes dramatic metabolic changes, encompassing not only the dissipation of energy-rich nutrients but also the *de novo* synthesis of new proteins, lipids and cellular organelles [1,33]. Thus, the thermogenic function of BAT requires an adaptive increase in proteasomal activity to secure cellular protein quality control. The UPS governs the degradation of 80—90% of intracellular proteins and serves as a fundamental mechanism for regulating cellular functions and maintaining protein homeostasis [34]. DUBs function to remove covalently attached ubiquitin from proteins, thereby controlling substrate activity and/or abundance [35,36]. In recent years, considerable evidence suggests that DUBs are involved in lipid metabolism [37—39]. However, few studies have elucidated the role of DUBs in regulating thermogenesis within adipose tissue. We initiated a data mining process on publicly accessible GEO databases. Among the 87 DUBs encoded by the mouse genome, USP2 stood out due to its significant upregulation during thermogenic activation.

USP2, a member of the ubiquitin-specific protease family, cleaves lysine-linked ubiquitin from substrate proteins, thereby preventing their proteasomal degradation [18]. For instance, USP2 deubiquitinates Aurora, an oncogenic serine/threonine kinase, consequently accelerating cell mitosis [40]. Additionally, USP2 interacts with and stabilizes mouse double minute 2 homologue (MDM2) [41], the epidermal growth factor receptor [42], and Cyclin A1 [43]. Indeed, accumulating evidence indicates that USP2 is pivotal in regulating energy metabolism in both physiological and pathological conditions. Lin's team reported that USP2 mediates the deubiquitylation of Cebpa and induces the expression of the 11β-hydroxysteroid dehydrogenase 1 (Hsd1) gene, thereby enhancing glucocorticoid signaling and stimulating hepatic gluconeogenesis [44]. Substrates of USP2 remaining unidentified, its presence in adipose tissue macrophages inhibits chronic inflammation in adipose tissue [20]. Within myoblasts, USP2 maintains OXPHOS and ATP supply, which may contribute to myoblast proliferation and myotube differentiation [45,46]. These studies suggest that USP2 may confer both beneficial and detrimental effects on metabolism. In our study, USP2 was found to promote the browning of white adipose tissue and enhance thermogenic function in brown adipose tissue. Our research fills the gap in the study of USP2, and more broadly DUBs, in adipose thermogenesis, and identified its substrate—EBF2, a key transcriptional regulator of brown fat cell fate and function.

EBF2 is a critical transcription factor belonging to the Early B-cell Factor (EBF) family, characterized by its unique DNA-binding domain and pivotal role in brown and beige adipose tissue development and function [47]. It regulates the expression of key thermogenic genes, including UCP1, and is essential for brown adipocyte specification, differentiation, as well as the browning of white adipose tissue [32,48,49]. Recent studies have elucidated its significant impact on energy expenditure and glucose homeostasis [50,51], underscoring its potential as a therapeutic target for metabolic disorders and its crucial role in maintaining overall metabolic health. Traditionally, the targeting of transcription factors has presented a significant challenge in the absence of specific ligands. The identification of protein degradation machinery represents a substantial advancement, as it offers an

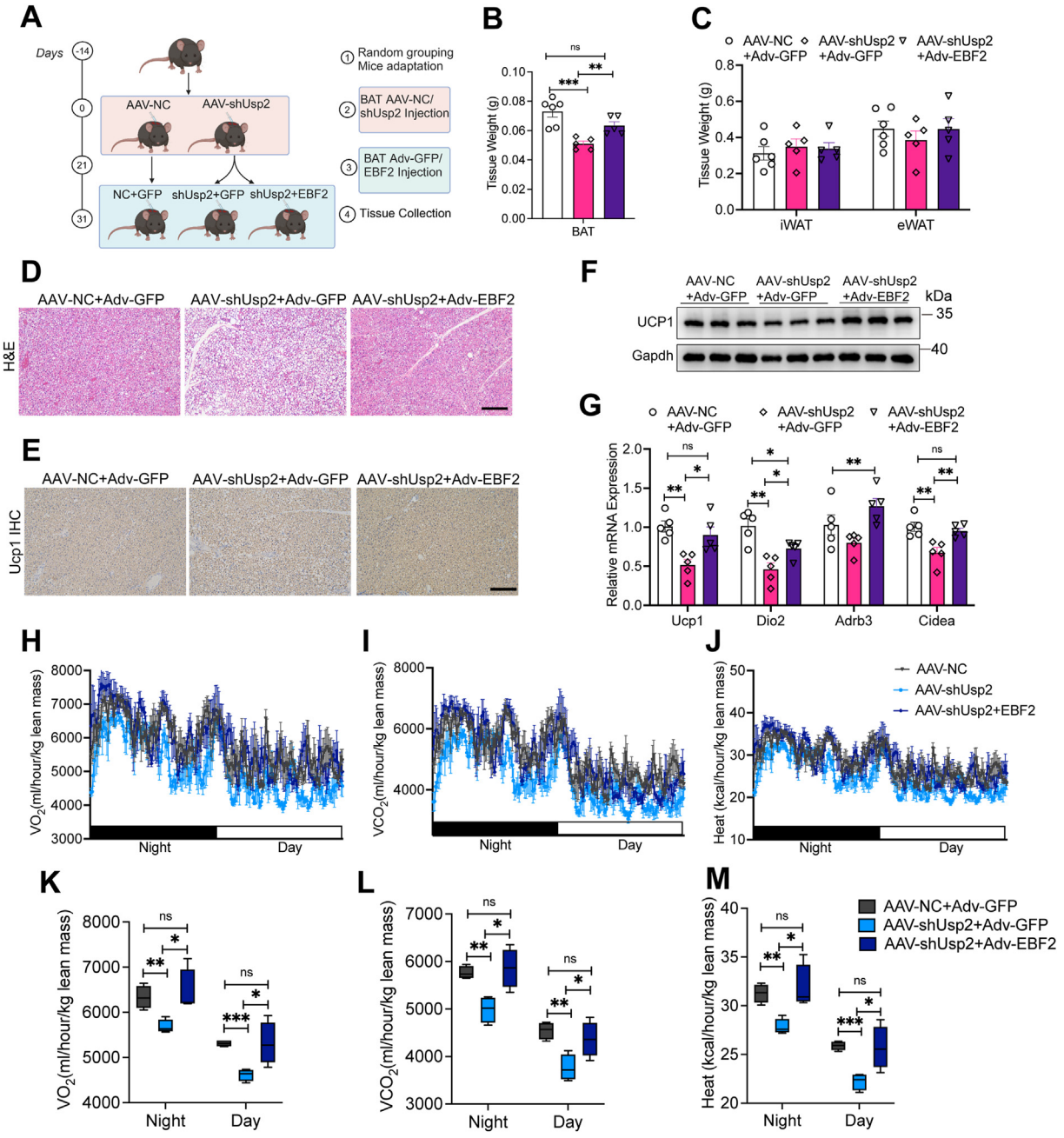

Figure 7: EBF2 overexpression attenuates USP2 deficiency-potentiated thermogenic dysfunction. A. Schematic illustration of the establishment of three groups: AAV-NC + Adv-GFP vs AAV-shUsp2 + Adv-GFP vs AAV-shUsp2 + Adv-EBF2, $n = 6$ vs 5 vs 5. Image created with BioRender.com. **B.** Tissue weight of BAT. **C.** Tissue weight of iWAT and eWAT. **D.** Representative H&E staining of BAT. **E.** Representative UCP1 immunostaining of BAT. **F.** Immunoblot analysis of UCP1. **G.** Quantitative PCR analysis of thermogenic genes of BAT ($n = 5$ vs 5 vs 5). **H-J.** Oxygen consumption rate (**H**), carbon dioxide production rate (**I**) and heat production rate (**J**) of mice over 24-hour period monitored at RT (22 °C) ($n = 4$ vs 4 vs 4). **K-M.** Average oxygen consumption rate (**K**), average carbon dioxide production rate (**L**) and average heat production rate (**M**) at day time or night time during the 24-hour of monitoring as in (H–J). For statistical analysis, two-way ANOVA was performed in H-J. Unpaired, two-tailed *t*-tests were performed in B, C, G and K-M. (*$P < 0.05$, **$P < 0.01$, ***$P < 0.001$). Each point represents a biological replicate. Data were presented as the mean ± S.E.M.

alternative approach to modulate specific transcriptional pathways of interest. Successful examples of this approach include the characterization of MDM2 for the p53 tumor suppressor protein [52] and Kelch-like ECH-associated protein 1 (KEAP1) for NF-E2 p45-related factor 2 (NRF2) [53]. Notably, in the context of adipose tissue, Cullin-2 (CUL2) has been identified for PR domain-containing 16 (PRDM16) [16]. Here we identified USP2 as the deubiquitinase that regulates EBF2 protein stability by catalyzing its polyubiquitination. Inhibition of the USP2—EBF2 axis significantly reduced the half-life of EBF2 protein and suppressed adipocyte thermogenesis. Notably, enhanced EBF2 protein stability, achieved through adipocyte-specific overexpression of USP2, mitigated diet-induced obesity, glucose intolerance, and insulin resistance in mice. These findings present a cell-autonomous approach for selectively activating the EBF2 pathway in adipose tissues, potentially offering new therapeutic strategies for metabolic disorders.

Our findings demonstrate that knockdown of USP2 in BAT not only increases lipid accumulation but also reduces BAT mass. Further analysis revealed that USP2 depletion significantly suppresses adipose thermogenesis while concurrently triggering apoptosis. Two independent studies in cancer cells have demonstrated that inhibition of USP2 and EBF2, respectively, enhances TRAIL-mediated apoptosis [54,55]. Of note, overexpression of EBF2 in BAT-specific USP2 knockdown mice not only reduced lipid droplet accumulation but also restored BAT mass, indicating that the dual effects of USP2 in BAT are at least partially mediated through the regulation of EBF2. In this study, we primarily focused on the critical role of USP2 in adipose thermogenesis, while its impact on apoptosis requires further investigation.

Meanwhile,the structural features of USP2 merit consideration when interpreting its role in BAT function. USP2 contains zinc-coordinating elements that may extend its functional repertoire beyond catalytic activity [18]. While the precise role of these structures in USP2 remains under investigation, studies of USP family proteins demonstrate that such domains can influence substrate specificity and protein interactions [56]. For instance, USP7 utilizes non-catalytic regions to regulate transcription factors and participate in metabolic gene regulation [57]. Similarly, Similarly, USP2 may directly modulate BAT thermogenesis-related gene expression through DNA binding or transcriptional regulation [58]. Future structure—function analyses are needed to determine whether USP2's zinc-coordinating structures contribute to the metabolic phenotypes in adipose thermogenesis.

Another limitation of this study is the unclear mechanism by which thermogenic activation upregulates USP2 expression in adipocytes. To explore this, we conducted preliminary predictions of *Usp2* promoter-binding transcription factors (TFs) via the transcription factor prediction website (http://genome.ucsc.edu/). Several TFs, such as HSF1, C/EBPβ, and c-Myc, were predicted to potentially regulate *Usp2* transcription. Given the fact that USP2 has multiple substrates in addition to EBF2, it will be interesting to further investigate other substrates that involve in fat metabolic homeostasis.

In summary, our findings revealed that USP2 plays a critical role in adipose thermogenic activation. BAT-specific knockdown or pharmacological inhibition of USP2 significantly impaired the thermogenic activity of brown adipocytes. Importantly, overexpression of USP2 in BAT ameliorated HFD-induced metabolic dysfunction. Mechanistically, we demonstrated that USP2 directly interacts with EBF2 and reduces K63-linked polyubiquitination of EBF2 at residue K321, subsequently enhancing the EBF2-mediated adaptive thermogenesis.

ACKNOWLEDGEMENT

This work was supported by Hainan Provincial Natural Science Foundation of China (821MS159). Innovative Research Team of High-level Local Universities in Shanghai (SHSMU-ZDCX20212700). National Natural Science Foundation of China (82370874).

CRediT AUTHORSHIP CONTRIBUTION STATEMENT

Yuejie Xu: Writing — review & editing, Writing — original draft, Visualization, Validation, Software, Resources, Project administration, Methodology, Investigation, Formal analysis, Data curation. **Ying Chen:** Visualization, Validation, Methodology, Formal analysis, Data curation, Conceptualization. **Ningning Bai:** Software, Resources, Methodology. **Yingying Su:** Validation, Resources, Data curation. **Yafen Ye:** Methodology, Investigation, Formal analysis. **Rong Zhang:** Software, Resources. **Ying Yang:** Resources, Methodology, Conceptualization. **Caizhi Liu:** Writing — review & editing, Visualization, Validation, Supervision, Resources, Methodology, Funding acquisition, Formal analysis, Data curation, Conceptualization. **Cheng Hu:** Writing — review & editing, Supervision, Resources, Funding acquisition, Formal analysis, Data curation, Conceptualization. **Jiemin Pan:** Writing — review & editing, Visualization, Validation, Supervision, Resources, Project administration, Methodology, Funding acquisition, Formal analysis, Data curation, Conceptualization.

DECLARATION OF COMPETING INTEREST

The authors declare that they have no known competing financial interests or personal relationships that could have appeared to influence the work reported in this paper.

DATA AVAILABILITY

Data will be made available on request.

APPENDIX A. SUPPLEMENTARY DATA

Supplementary data to this article can be found online at https://doi.org/10.1016/j.molmet.2025.102139.

REFERENCES

[1] Cannon B, Nedergaard J. Brown adipose tissue: function and physiological significance. Physiol Rev 2004;84(1):277—359.
[2] Cypess AM, Lehman S, Williams G, Tal I, Rodman D, Goldfine AB, et al. Identification and importance of brown adipose tissue in adult humans. N Engl J of Med 2009;360(15):1509—17.
[3] Harms M, Seale P. Brown and beige fat: development, function and therapeutic potential. Nat Med 2013;19(10):1252—63.
[4] Cohen P, Kajimura S. The cellular and functional complexity of thermogenic fat. Nat Rev Mol Cell Biol 2021;22(6):393—409.
[5] Wolfrum C, Gerhart-Hines Z. Fueling the fire of adipose thermogenesis. Science 2022;375(6586):1229—31.
[6] van Marken Lichtenbelt WD, Vanhommerig JW, Smulders NM, Drossaerts JM, Kemerink GJ, Bouvy ND, et al. Cold-activated brown adipose tissue in healthy men. N Engl J Med 2009;360(15):1500—8.
[7] Feldmann HM, Golozoubova V, Cannon B, Nedergaard J. UCP1 ablation induces obesity and abolishes diet-induced thermogenesis in mice exempt from thermal stress by living at thermoneutrality. Cell Metab 2009;9(2):203—9.
[8] Rothwell NJ, Stock MJ. A role for brown adipose tissue in diet-induced thermogenesis. Obes Res 1997;5(6):650—6.
[9] Varshavsky A. The ubiquitin system, an immense realm. Annu Rev Biochem 2012;81:167—76.
[10] Celebi G, Kesim H, Ozer E, Kutlu O. The effect of dysfunctional ubiquitin enzymes in the pathogenesis of Most common diseases. Int J Mol Sci 2020;21(17):6335.
[11] Clague MJ, Barsukov I, Coulson JM, Liu H, Rigden DJ, Urbé S. Deubiquitylases from genes to organism. Physiol Rev 2013;93(3):1289—315.
[12] Li Y, Reverter D. Molecular mechanisms of DUBs regulation in signaling and disease. Int J Mol Sci 2021;22(3).
[13] Coyne ES, Bédard N, Gong YJ, Faraj M, Tchernof A, Wing SS. The deubiquitinating enzyme USP19 modulates adipogenesis and potentiates high-fat-diet-induced obesity and glucose intolerance in mice. Diabetologia 2019;62(1):136—46.
[14] Gao Y, Koppen A, Rakhshandehroo M, Tasdelen I, Van De Graaf SF, Van Loosdregt J, et al. Early adipogenesis is regulated through USP7-mediated deubiquitination of the histone acetyltransferase TIP60. Nat Commun 2013;4:2656.

[15] Kim MS, Baek JH, Lee J, Sivaraman A, Lee K, Chun KH. Deubiquitinase USP1 enhances CCAAT/enhancer-binding protein beta (C/EBPβ) stability and accelerates adipogenesis and lipid accumulation. Cell Death Dis 2023;14(11):776.
[16] Wang Q, Li H, Tajima K, Verkerke AR, Taxin ZH, Hou Z, et al. Post-translational control of beige fat biogenesis by PRDM16 stabilization. Nature 2022;609(7925):151—8.
[17] Jeon YG, Nahmgoong H, Oh J, Lee D, Kim DW, Kim JE, et al. Ubiquitin ligase RNF20 coordinates sequential adipose thermogenesis with brown and beige fat-specific substrates. Nat Commun 2024;15(1):940.
[18] Renatus M, Parrado SG, D'Arcy A, Eidhoff U, Gerhartz B, Hassiepen U, et al. Structural basis of ubiquitin recognition by the deubiquitinating protease USP2. Structure 2006;14(8):1293—302.
[19] Kitamura H, Hashimoto M. USP2-Related cellular signaling and consequent pathophysiological outcomes. Int J Mol Sci 2021;22(3):1209.
[20] Saito N, Kimura S, Miyamoto T, Fukushima S, Amagasa M, Shimamoto Y, et al. Macrophage ubiquitin-specific protease 2 modifies insulin sensitivity in obese mice. Biochem Biophys Rep 2017;9:322—9.
[21] Graner E, Tang D, Rossi S, Baron A, Migita T, Weinstein LJ, et al. The isopeptidase USP2a regulates the stability of fatty acid synthase in prostate cancer. Cancer Cell 2004;5(3):253—61.
[22] Cypess AM, White AP, Vernochet C, Schulz TJ, Xue R, Sass CA, et al. Anatomical localization, gene expression profiling and functional characterization of adult human neck brown fat. Nat Med 2013;19(5):635—9.
[23] Bai N, Ma J, Alimujiang M, Xu J, Hu F, Xu Y, et al. Bola3 regulates beige adipocyte thermogenesis via maintaining mitochondrial homeostasis and lipolysis. Front Endocrinol 2021;11:592154.
[24] Jimenez V, Jambrina C, Casana E, Sacristan V, Muñoz S, Darriba S, et al. FGF21 gene therapy as treatment for obesity and insulin resistance. EMBO Mol Med 2018;10(8):e8791.
[25] Jimenez V, Muñoz S, Casana E, Mallol C, Elias I, Jambrina C, et al. In vivo adeno-associated viral vector-mediated genetic engineering of white and brown adipose tissue in adult mice. Diabetes 2013;62(12):4012—22.
[26] Johansen OS, Ma T, Hansen JB, Markussen LK, Schreiber R, Reverte-Salisa L, et al. Lipolysis drives expression of the constitutively active receptor GPR3 to induce adipose thermogenesis. Cell 2021;184(13):3502—18. e3533.
[27] Tseng YH, Kriauciunas KM, Kokkotou E, Kahn CR. Differential roles of insulin receptor substrates in brown adipocyte differentiation. Mol Cell Biol 2004;24(5):1918—29.
[28] Bu D, Luo H, Huo P, Wang Z, Zhang S, He Z, et al. KOBAS-i: intelligent prioritization and exploratory visualization of biological functions for gene enrichment analysis. Nucleic Acids Res 2021;49(W1):W317—25.
[29] Mina AI, LeClair RA, LeClair KB, Cohen DE, Lantier L, Banks AS. CalR: a web-based analysis tool for indirect calorimetry experiments. Cell Metab 2018;28(4):656—66. e651.
[30] Davis MI, Pragani R, Fox JT, Shen M, Parmar K, Gaudiano EF, et al. Small molecule inhibition of the ubiquitin-specific protease USP2 accelerates cyclin D1 degradation and leads to cell cycle arrest in colorectal cancer and mantle cell lymphoma models. J Biol Chem 2016;291(47):24628—40.
[31] Alvarez-Dominguez JR, Bai Z, Xu D, Yuan B, Lo KA, Yoon MJ, et al. De novo reconstruction of adipose tissue transcriptomes reveals long non-coding RNA regulators of brown adipocyte development. Cell Metab 2015;21(5):764—76.
[32] Rajakumari S, Wu J, Ishibashi J, Lim HW, Giang AH, Won KJ, et al. EBF2 determines and maintains brown adipocyte identity. Cell Metab 2013;17(4):562—74.
[33] Saito M, Okamatsu-Ogura Y, Matsushita M, Watanabe K, Yoneshiro T, Nio-Kobayashi J, et al. High incidence of metabolically active brown adipose tissue in healthy adult humans: effects of cold exposure and adiposity. Diabetes 2009;58(7):1526—31.
[34] Nandi D, Tahiliani P, Kumar A, Chandu D. The ubiquitin-proteasome system. J Biosci 2006;31:137—55.
[35] Clague MJ, Coulson JM, Urbé S. Cellular functions of the DUBs. J Cell Sci 2012;125(2):277—86.
[36] Snyder NA, Silva GM. Deubiquitinating enzymes (DUBs): regulation, homeostasis, and oxidative stress response. J Biol Chem 2021;297(3).
[37] Vogel K, Bläske T, Nagel MK, Globisch C, Maguire S, Mattes L, et al. Lipid-mediated activation of plasma membrane-localized deubiquitylating enzymes modulate endosomal trafficking. Nat Commun 2022;13(1):6897.
[38] Dubiel D, Bintig W, Kähne T, Dubiel W, Naumann M. Cul3 neddylation is crucial for gradual lipid droplet formation during adipogenesis. Biochim Biophys Acta Mol Cell Res 2017;1864(8):1405—12.
[39] Suzuki M, Setsuie R, Wada K. Ubiquitin carboxyl-terminal hydrolase l3 promotes insulin signaling and adipogenesis. Endocrinology 2009;150(12):5230—9.
[40] Shi Y, Solomon LR, Pereda-Lopez A, Giranda VL, Luo Y, Johnson EF, et al. Ubiquitin-specific cysteine protease 2a (USP2a) regulates the stability of Aurora-A. J Biol Chem 2011;286(45):38960—8.
[41] Stevenson LF, Sparks A, Allende-Vega N, Xirodimas DP, Lane DP, Saville MK. The deubiquitinating enzyme USP2a regulates the p53 pathway by targeting Mdm2. EMBO J 2007;26(4):976—86.
[42] Liu Z, Zanata SM, Kim J, Peterson MA, Di Vizio D, Chirieac LR, et al. The ubiquitin-specific protease USP2a prevents endocytosis-mediated EGFR degradation. Oncogene 2013;32(13):1660—9.
[43] Kim J, Kim WJ, Liu Z, Loda M, Freeman MR. The ubiquitin-specific protease USP2a enhances tumor progression by targeting cyclin A1 in bladder cancer. Cell Cycle 2012;11(6):1123—30.
[44] Molusky MM, Li S, Ma D, Yu L, Lin JD. Ubiquitin-specific protease 2 regulates hepatic gluconeogenesis and diurnal glucose metabolism through 11β-hydroxysteroid dehydrogenase 1. Diabetes 2012;61(5):1025—35.
[45] Kitamura H, Fujimoto M, Hashimoto M, Yasui H, Inanami O. USP2 mitigates reactive oxygen species—induced mitochondrial damage via UCP2 expression in myoblasts. Int J Mol Sci 2024:25.
[46] Hashimoto M, Saito N, Ohta H, Yamamoto K, Tashiro A, Nakazawa K, et al. Inhibition of ubiquitin-specific protease 2 causes accumulation of reactive oxygen species, mitochondria dysfunction, and intracellular ATP decrement in C2C12 myoblasts. Physiol Rep 2019;7(14):e14193.
[47] Liao D. Emerging roles of the EBF family of transcription factors in tumor suppression. Mol Cancer Res 2009;7(12):1893—901.
[48] Stine RR, Shapira SN, Lim HW, Ishibashi J, Harms M, Won KJ, et al. EBF2 promotes the recruitment of beige adipocytes in white adipose tissue. Mol Metabol 2016;5(1):57—65.
[49] Wang W, Kissig M, Rajakumari S, Huang L, Lim HW, Won KJ, et al. Ebf2 is a selective marker of brown and beige adipogenic precursor cells. Proc Natl Acad Sci 2014;111(40):14466—71.
[50] Shapira SN, Lim H-W, Rajakumari S, Sakers AP, Ishibashi J, Harms MJ, et al. EBF2 transcriptionally regulates brown adipogenesis via the histone reader DPF3 and the BAF chromatin remodeling complex. Genes Dev 2017;31(7):660—73.
[51] Shao M, Zhang Q, Truong A, Shan B, Vishvanath L, Li L, et al. ZFP423 controls EBF2 coactivator recruitment and PPARγ occupancy to determine the thermogenic plasticity of adipocytes. Genes Dev 2021;35(21—22):1461—74.
[52] Vassilev LT, Vu BT, Graves B, Carvajal D, Podlaski F, Filipovic Z, et al. In vivo activation of the p53 pathway by small-molecule antagonists of MDM2. Science 2004;303(5659):844—8.
[53] Cuadrado A, Rojo AI, Wells G, Hayes JD, Cousin SP, Rumsey WL, et al. Therapeutic targeting of the NRF2 and KEAP1 partnership in chronic diseases. Nat Rev Drug Discov 2019;18(4):295—317.

[54] Lee TG, Woo SM, Seo SU, Kim S, Park JW, Chang YC, Kwon TK. Inhibition of USP2 enhances TRAIL-mediated cancer cell death through downregulation of survivin. Int J Mol Sci 2023;24(16).

[55] Patiño-García A, Zalacain M, Folio C, Zandueta C, Sierrasesúmaga L, San Julián M, et al. Profiling of chemonaive osteosarcoma and paired-normal cells identifies EBF2 as a mediator of osteoprotegerin inhibition to tumor necrosis factor-related apoptosis-inducing ligand-induced apoptosis. Clin Cancer Res 2009;15(16):5082–91.

[56] Bonnet J, Romier C, Tora L, Devys D. Zinc-finger UBPs: regulators of deubiquitylation. Trends Biochem Sci 2008;33(8):369–75.

[57] Ni W, Lin S, Bian S, Zheng W, Qu L, Fan Y, et al. USP7 mediates pathological hepatic de novo lipogenesis through promoting stabilization and transcription of ZNF638. Cell Death Dis 2020;11(10):843.

[58] Tencer AH, Liang Q, Zhuang Z. Divergence in ubiquitin interaction and catalysis among the ubiquitin-specific protease family deubiquitinating enzymes. Biochemistry 2016;55(33):4708–19.

